Carotenoids co-localize with hydroxyapatite, cholesterol, and other lipids in calcified stenotic aortic valves. *Ex vivo* Raman maps compared to histological patterns

A. Bonetti,[1] A. Bonifacio,[2] A. Della Mora,[1] U. Livi,[1] M. Marchini,[1] F. Ortolani[1]

[1]Department of Experimental and Clinical Medicine, University of Udine
[2]Department of Engineering and Architecture, University of Trieste, Italy

Abstract

Unlike its application for atherosclerotic plaque analysis, Raman microspectroscopy was sporadically used to check the sole nature of bioapatite deposits in stenotic aortic valves, neglecting the involvement of accumulated lipids/lipoproteins in the calcific process. Here, Raman microspectroscopy was employed for examination of stenotic aortic valve leaflets to add information on nature and distribution of accumulated lipids and their correlation with mineralization in the light of its potential precocious diagnostic use. Cryosections from surgically explanted stenotic aortic valves (n=4) were studied matching Raman maps against specific histological patterns. Raman maps revealed the presence of phospholipids/triglycerides and cholesterol, which showed spatial overlapping with one another and Raman-identified hydroxyapatite. Moreover, the Raman patterns correlated with those displayed by both von-Kossa-calcium- and Nile-blue-stained serial cryosections. Raman analysis also provided the first identification of carotenoids, which co-localized with the identified lipid moieties. Additional fit concerned the distribution of collagen and elastin. The good correlation of Raman maps with high-affinity staining patterns proved that Raman microspectroscopy is a reliable tool in evaluating calcification degree, alteration/displacement of extracellular matrix components, and accumulation rate of different lipid forms in calcified heart valves. In addition, the novel identification of carotenoids supports the concept that valve stenosis is an *atherosclerosis-like valve lesion*, consistently with their previous Raman microspectroscopical identification inside atherosclerotic plaques.

Introduction

Calcific aortic valve stenosis (CAVS) still represents the leading indication for valve replacement in aging Western populations. CAVS shares clinical and histopathological features with atherosclerosis,[1-3] leading to the increasingly accepted concept that these two diseases may represent the same disorder occurring in different anatomical sites.[4,5] Notably, in both stenotic valves[2,3] and atherosclerotic plaques[6,7] calcium salt precipitation on accumulated cholesterol has been reported as a distinctive event. What cause-and-effect relationship may exist between the presence of this neutral lipid and calcium salt nucleation is yet to be exhaustively elucidated, in contrast with the more easily conceivable involvement of negatively charged phospholipids (PLs) in pathological biomineralization processes. Consistently, cell-membrane-derived acidic PLs have been identified as major calcium nucleator in both CAVS[8,9] and atherosclerosis.[10] In addition, using the procalcific subdermal model, PL involvement has been ultrastructurally shown in the context of a peculiar degenerative process affecting aortic valve interstitial cells (AVICs), in which the crucial event was a progressive colliquation of all cell membranes, culminating with the generation of an acidic-PL-rich material outlining dying cells or their remnants and acting as a major hydroxyapatite (HA) nucleator.[11-14] Similar cell degeneration has also been shown to concern AVICs in *in vitro* models simulating dystrophic[15] and metastatic[16] calcification. Raman microspectroscopy is an analytical technique measuring the characteristic molecular vibrations of various chemical groups after irradiation with a laser beam.[17] Using this technique, HA, cholesterol, and carotenoids have been identified within atherosclerotic plaques,[18-20] whereas identification of HA solely has been reported for stenotic aortic valves.[21,22]

The present investigation was aimed to better characterize tissue alterations and parallel accumulation of HA and different lipids in CAVS-affected aortic valve leaflets as well as evaluate whether Raman microspectroscopy can be concerned as a potential diagnostic tool, by matching the achieved *ex vivo* Raman maps against specific histological patterns. Raman maps of HA, PLs/triglycerides (PLs/TGs), cholesterol, and carotenoids exhibited spatial overlapping with one another and histological patterns, besides providing the novel identification of carotenoids in these calcific valves.

Correspondence: Prof. Fulvia Ortolani, Department of Experimental and Clinical Medicine, University of Udine, Piazzale Kolbe 3, I-33100, Udine, Italy.
Tel. +39.0432.494242 - Fax: +39.0432.494201.
E-mail: fulvia.ortolani@uniud.it

Key words: Valve calcification, stenosis, carotenoids, lipids, Raman microspectroscopy.

Contributions: all authors contributed equally.

Conflict of interest: the authors declare no conflict of interest.

Received for publication: 20 January 2015.
Accepted for publication: 5 March 2015.

European Journal of Histochemistry 2015; 59:2505
doi:10.4081/ejh.2015.2505

Materials and Methods

Sampling and initial processing

Native, tricuspid aortic valves were surgically explanted from patients (n=4; mean age 78±8 years) subjected to cardiac valve replacement at the Cardiothoracic Surgery Unit of the University Hospital of Udine. The present investigation was approved by the Internal Review Board (IRB) of the Department of Experimental and Clinical Medicine so human studies have been performed in accordance with the ethical standards laid down in the 1964 Declaration of Helsinki and its later amendments. Informed consent allowing aortic valve use for experimental purposes was signed by all patients prior to their inclusion in the study. All aortic valves were affected by severe, non-rheumatic stenosis as diagnosed by pre-operative clinical and echocardiographic parameters (valve area <1 cm^2; middle transvalvular gradient >65 mmHg). After explantation, aortic valves were immersed in sterile 0.9% NaCl solution and their leaflets were excised and subdivided into two hemicusps by cutting them along the middle longitudinal axis. For each patient, one hemi-cusp was cooled by dipping into 2-methylbutane liquid for subsequent Raman and histological analyses, being the other one formalin-fixed for routinary hematoxylin&eosin staining.

Cryosectioning

For each cooled hemi-cusp, three 1.5-mm-spaced, 15-μm-thick cryosections (n=12) were longitudinally cut, mounted on CaF_2 slides, air-dried, and stored at -20°C for subsequent Raman microspectroscopic examination. Additional serial and para-serial 8-μm-thick cryosections were mounted on glass slides, air-dried, and fixed with phosphate-buffered 5% formaldehyde for subsequent histological staining, as described below.

Raman microspectroscopy

Raman maps were collected in back scattering geometry using the Renishaw InVia Raman microscope equipped with a 785 nm diode laser delivering 170mW of laser power at the sample. A 785 nm near infrared wavelength was used to limit tissue autofluorescence, which should interfere with Raman spectrum measurements. The CaF_2 slide supporting the tissue sections was mounted on a ProScan II motorized stage (Prior, Cambridge, UK) under the microscope. A Leica 50 microscope objective (N.A. 0.85) focused the laser on the sample. A 1200 L/mm grating yielded a spectral resolution of 4 cm^{-1}. A thermoelectrically cooled charge coupled device (CCD) camera was used for detection. The spectrograph was calibrated using the lines of a Ne lamp. Mapping was achieved collecting spectra with steps of 12 μm, with 10 sec exposure time for each spectrum, for a total of 5708 spectra, each consisting of 1203 data points. Spectra were obtained in the 600-1800 cm^{-1} region using the synchro mode of the instrument software WiRE™ 3.2 (Renishaw), in which the grating is continuously moved to obtain Raman spectra of extended spectral regions. Data preprocessing and analysis were carried out using the hyperSpec package (Beleites and Sergo, hyperSpec: a package to handle hyperspectral data sets in R; http://hyperspec.r-forge.r-project.org/).

High-affinity histological staining

von Kossa staining

Serial cryosections were treated with 1% silver nitrate solution for 15 min, with exposure to direct sunlight, and 5% sodium thiosulfate reducing solution for 5 min. Cryosections were then weakly counterstained with hematoxylin and eosin, dehydrated in graded ethanols, cleared with xylene, and mounted with Eukitt® mounting medium.

Movat staining

Para-serial cryosections were stained with 1% alcian blue acidic solution for 40 min, differentiated in 0.3% sodium carbonate solution for 2 h, and then incubated with i) Weigert's resorcin-fuchsin solution for 40 min; ii) celestine blue solution for 5 min; iii) Weigert's iron hematoxylin for 10 min; and iv) van Gieson solution for 5 min. Dehydration and mounting were as described above.

Nile blue staining

Para-serial cryosections were stained with 1% Nile blue solution at 60°C for 5 min, differentiated in warm 1% acetic acid solution, and mounted with glycerol mounting medium. Discrimination between neutral lipids and acidic lipids is allowed because the used dye is a mixture of oxazone (Nile red) and oxazine sulphate (Nile blue), in that the former is mainly dissolved by neutral lipids and the latter by acidic ones. Observation and recording were made using a Zeiss AxioImager photomicroscope.

Results

Figure 1 shows the Raman spectrum calculated as the average of all intensity-normalized spectra collected in the map from a representative CAVS-affected valve leaflet cryosection. All the bands usually observed in Raman spectra of biological tissues were detected, such as the sharp and intense band at 1004 cm^{-1} assigned to the phenylalanine ring vibration, the bands at 1250-1270 cm^{-1} and 1600-1700 cm^{-1} assigned to amide I and III vibrational modes respectively, and the bands at 1400-1500 cm^{-1} assigned to $-CH_2-$ and $-CH_3$ deformation modes. Characteristic spectral peaks were also detected of type B carbonate HA at 959 cm^{-1}, collagen at 877, 922, and 939 cm^{-1}, elastin at 1103 and 1340 cm^{-1}, PLs/TGs at 719 and 1738 cm^{-1}, cholesterol at 700 and 741 cm^{-1}, and carotenoids at 1159 and 1527 cm^{-1}. The presence of unsaturated lipids was inferred from the small, but still distinguishable, peak at 1660 cm^{-1} superimposing to the broad amide I protein peak. Peaks at 1064 and 1128 cm^{-1} indicated the presence of saturated fatty acid chains.[23] All spectra collected from the other cryosections revealed the presence of the same chemical species, although showing slight changes in their peak intensities (*not shown*).

The measured Raman intensities were further converted into *chemical images* displaying the relative concentrations of the chemical species identified in the analyzed valve leaflet cross cryosections side-by-side, so including all three layers called *tunica fibrosa*, *tunica spongiosa*, and *tunica ventricularis*, in which major tissue alterations were detectable in the *fibrosa* layer (Figure 2 A-C and G-I). The expression *relative concentrations* means that in each image color scales span minimum to maximum concentration values of the chemical species in its own map, so they cannot be quantitatively compared to each other. The Raman map of HA (Figure 2A) showed the highest intensity to coincide exactly with the brown calcific nodule recognizable on the serial cryosection subjected to von Kossa silver staining (Figure 2D). Lower HA intensity resulted for two pseudo-triangle-shaped areas

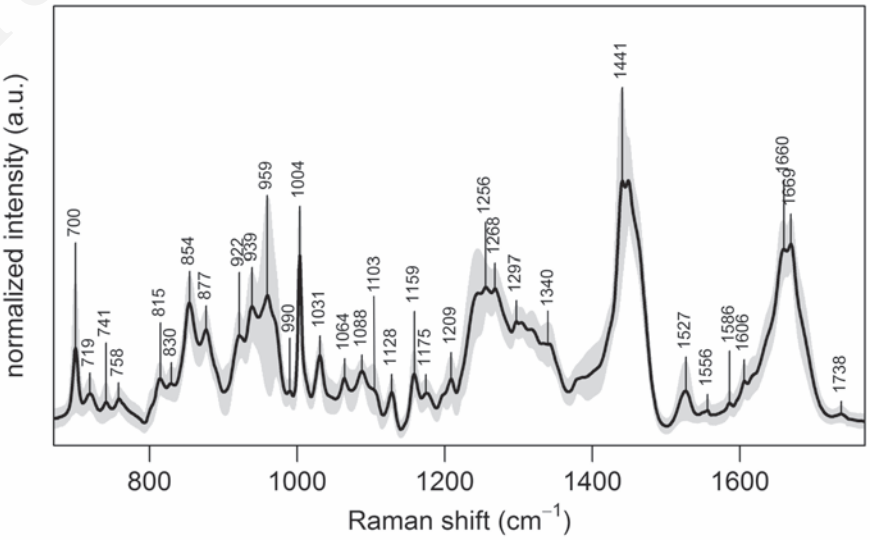

Figure 1. Mean Raman spectrum of the Raman map collected from a representative CAVS-affected valve leaflet cryosection, calculated over all the 5708 spectra of the map. Intensity standard deviation, showing the spectral variability, is shown in light grey. For all spectra, excitation wavelength was at 785 nm, laser power was 170 mW, and acquisition time was 10 seconds.

in the *fibrosa* layer referred to below as T1 and T2, the former enveloping the calcific nodule and the latter located above. Additional very high intensity was exhibited by random one-pixel-wide spots located in T1. Also these spots roughly correlated with the punctate silver precipitates showed by the von-Kossa-stained cryosection inside the corresponding area. In contrast, the HA Raman map showed a mutual exclusion pattern as opposed to those of collagen (Figure 2B) and elastin (Figure 2C), since the areas showing higher mineral intensity were superimposable to those of lower intensity of the two extracellular matrix fibrous components. In turn, Raman patterns of the latter were roughly consistent with their distribution on histological cryosections, revealing both fibrous components by eosin on the counterstained von-Kossa-reacted cryosection (Figure 2D) as well as collagen in red and elastin in dark brown on the Movat-stained cryosection (Figure 2E). Further fitting resulted for the maps of the three lipid moieties identified, which were closely superimposable to each other (Figure 2 G-I). In addition, the areas showing intermediate intensity of PLs/TGs (Figure 2G), cholesterol (Figure 2H), and carotenoids (Figure 2I) correlated with both T1 and T2 areas in the HA map, including the presence of single or clustered one-pixel-wide spots with high intensity. Surprisingly, there was the exception that lipid maps showed minimal intensity just in the area exhibiting the highest intensity in the HA map, i.e. the calcific nodule, although some intranodular intensity appeared for PLs/TGs. Raman maps of lipids were also roughly consistent with the histological patterns shown by the cryosection subjected to Nile blue lipid staining (Figure 2F), since a red-stained triangle-shaped area, indicating the presence of neutral lipids, corresponded to T1 on lipid Raman maps and single or clustered blue-stained punctate sites, indicating the presence of acidic lipids, were scattered inside this T1-like area correlating with topical high Raman intensity of PLs/TGs. In contrast, a T2-like area was not shown by the histological counterpart. On the other hand, prominent Nile blue staining was apparent at the calcific nodule edge, preserved from artifactual detachment. All Raman maps concerning the other cryosections were consistent with the histological counterparts, although they showed different topographical distributions of the identified chemical species (*not shown*).

Discussion

The present investigation showed that good consistency exists between Raman maps and specific histological patterns derived from cryosections of CAVS-affected valve leaflets, leading to conclude that this vibrational microspectroscopy represents a reliable technique to identify unknown chemical species or validate those revealed by high-affinity histological procedures. Combining these two approaches, the identification, typization, and localization of HA and distinct lipid forms were the major outcomes. In particular, HA Raman maps showed the highest mineral intensity to correspond exactly to calcific nodules on the histological counterpart. As inferred from the Raman shift of the $\nu_1PO_4^{3-}$ band at 959 cm^{-1}, the precipitated mineral was type B carbonate HA,[24] as recently reported using the same technique.[21,22] Taking into account that type B carbonate HA represents the most abundant form of bioapatite in young bones,[25] the present

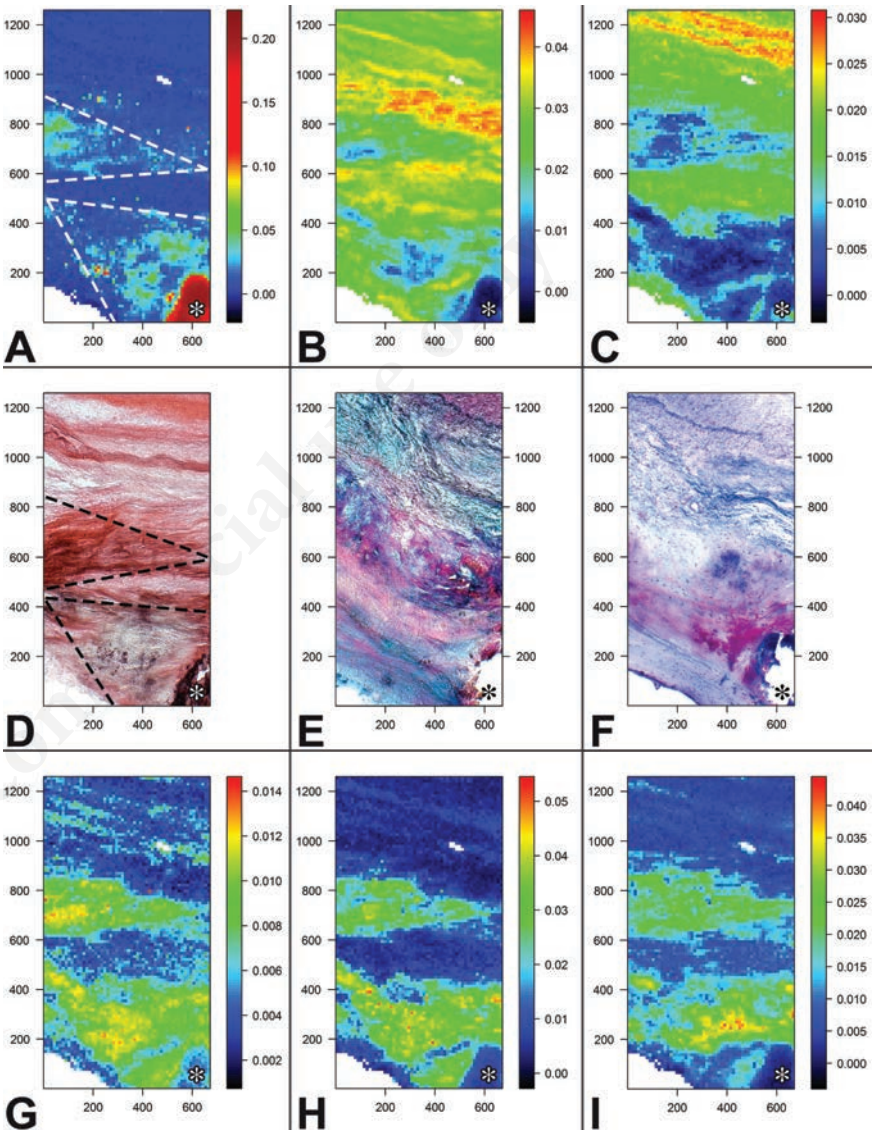

Figure 2. Images obtained from the Raman map showing the total normalized intensity of A) hydroxyapatite peak (959 cm^{-1}); B) collagen peaks (877, 922, and 939 cm^{-1}); C) elastin peaks (1103 and 1340 cm^{-1}); G) phospholipid/triglyceride peaks (719 and 1738 cm^{-1}); H) cholesterol peaks (700 and 741 cm^{-1}); I) carotenoid peaks (1159 and 1527 cm^{-1}). Color scale bars refer to arbitrary units of total normalized intensities. Histological pictures obtained from D) a serial cryosection subjected to von Kossa calcium staining and para-serial cryosections stained with E) Movat pentachrome method for extracellular matrix components or F) Nile blue method for neutral and acidic lipids. Two triangle-shaped regions are outlined (dashed lines in A and D) in which correlating features can be appreciated; these regions are promptly recognizable in all Raman images (A-C and G-I) and are referred as T1 and T2 regions in the text. A calcific nodule portion (asterisk) is displayed in the lower right corner. Histological slide original magnification: 5x. Abscissa and ordinate values are expressed in μm.

result might be consistent with heterotopic ossification taking place in CAVS. However, it should be emphasized that i) bone-formed territories were never histologically encountered in this investigation; and ii) bone metaplasia was reported to be associated with dystrophic calcification in less than 13% of hundreds of aortic valves and dozens of mitral valves.[26,27] Such a specification is needed because valve calcification is often misconceived as valve ossification instead of considering this latter as an alternative, minority pro-calcific event.

Besides showing marked co-localization of the three moieties identified, Raman maps of lipids were also found to be consistent with lipid distribution in the histological counterpart. Major fitting concerned the good superimposability of T1 in the cholesterol Raman map with the neutral-lipid-rich red area in the Nile-blue-stained cryosection. In the latter, some parallelism between the distribution of acidic-lipid-rich blue punctate sites and that of very intense one-pixel-wide spots inside T1 in the PL/TG Raman map resulted as well. However, there were also some inconsistencies, the most apparent being the lack of a T2-like area in the histological counterpart. It should be kept in mind that uncontrollable events can affect reliability and reproducibility of the patters supplied by this high-affinity staining, depending on heterogeneous dye-to-substratum affinities and not steady stain-to-stain competition degrees. The existence of further consistency between the lipid Raman maps and that of HA supports the finding that lipid accumulation closely correlates with priming of biomineralization, in spite of the *prima facie* contradictory very low lipid intensity just at level of the calcific nodule. Likely, this conflicting result can be ascribed to a masking effect exerted by the overwhelming precipitation of HA crystals at the level of this prominently calcified area. Taking into account that i) PLs/TGs were the sole lipid moiety showing some intensity inside the calcific nodule area; and ii) prominent Nile blue staining was apparent at calcific nodule edges, the concept supported is that a major role in HA crystal precipitation is played by PLs, consistent with reports on ectopic calcification including *in vivo* pathological conditions[8,9] as well as experimental ones using *in vivo*[11–14] and *in vitro*[15,16] models. The microspectroscopic identification of cholesterol in mineralizing areas is consistent with neutral lipid accumulation representing a distinctive feature of CAVS,[2,3] in which oxidized cholesterol might contribute to valve mineralization.[28]

To our knowledge, this study provided the first-time identification of carotenoids in stenotic valve leaflets, besides revealing their co-accumulation with the other lipid forms at valve mineralizing areas. Being carotenoids transported in the human plasma by LDLs together with cholesterol,[29] it might be assumed that LDL-cholesterol-carotenoid complexes are phagocytized by lipid-loading macrophages and AVICs during the early stages of CAVS. Since Raman microspectroscopy already revealed the presence of carotenoids as well as their co-localization with lipid deposits in atherosclerotic plaques,[18–20] the concept is supported that CAVS represents a type of *valve atherosclerosis*,[4,5] with progressive LDL entering and lipid-laden cell degeneration/death being shared features in these two types of cardiovascular diseases. Taking also into account that i) carotenoids can be revealed very easily because of their very intense spectral peaks, and ii) Raman spectra were already obtained *in vivo* by shining the laser beam upon artery wall atherosclerotic lesions via miniaturized fiber-optical probes,[30,31] it is worth noting that the *in vivo* microspectroscopic identification of carotenoids might be usefully exploited to improve the poor capability of a precocious CAVS diagnosis.

Good consistency between Raman maps and histological patterns resulted also for collagen distribution, since mapped areas showing very low collagen intensity roughly corresponded to those completely lacking in eosinophilia in the histological counterpart. Since the same areas in turn roughly corresponded to those with very high HA intensity, it is feasible that in valve mineralizing areas degeneration of collagen fibers may take place, consistent with inflammation-dependent release of matrix metalloproteinases by resident AVICs.[3]. Additional consistency concerned elastin distribution since both the Raman map and the Movat-stained para-serial cryosection showed this protein to be mainly present in the *ventricularis* layer, consistent with native valve leaflet structure as well as the fact that this valve region usually retains its normal features remaining free from mineralization.[2]

In conclusion, Raman maps added information on the presence and topographical distribution of precipitated calcium, accumulated lipids including cholesterol/carotenoids, and altered extracellular matrix components in CAVS-affected valve leaflets. Moreover, Raman microspectroscopy was found to represent a potential technique to investigate *in vivo* the alterations anticipating or characterizing this *atherosclerosis-like valve disease*."

References

1. Stewart BF, Siscovick D, Lind BK, Gardin JM, Gottdiener JS, Smith VE et al. Clinical factors associated with calcific aortic valve disease. Cardiovascular Health Study. J Am Coll Cardiol 1997;29:630-4.
2. Otto CM, Kuusisto J, Reichenbach DD, Gown AM, O'Brien KD. Characterization of the early lesion of "degenerative" valvular aortic stenosis. Histological and immunohistochemical studies. Circulation 1994; 90:844-53.
3. O'Brien KD, Reichenbach DD, Marcovina SM, Kuusisto J, Alpers CE, Otto CM. Apolipoproteins B, (a), and E accumulate in the morphologically early lesion of "degenerative" valvular aortic stenosis. Arterioscler Thromb Vasc Biol 1996; 16:523-32.
4. Agmon Y, Khandheria BK, Miessner I, Sicks JR, O'Fallon WM, Wiebers DO et al. Aortic valve sclerosis and aortic atherosclerosis: different manifestations of the same disease? Insights from a population-based study. J Am Coll Cardiol 2001; 38:827-34.
5. Kuusisto J, Räsänen K, Särkioja T, Alarakkola E, Kosma VM. Atherosclerosis-like lesions of the aortic valve are common in adults of all ages: a necropsy study. Heart 2005;91:576-82.
6. Hirsch D, Azoury R, Sarig S, Kruth HS. Colocalization of cholesterol and hydroxyapatite in human atherosclerotic lesions. Calcif Tissue Int 1993;52:94-8.
7. Sarig, S, Weiss TA, Katz I, Kahana F, Azoury R, Okon E et al. Detection of cholesterol associated with calcium mineral using confocal fluorescence microscopy. Lab Invest 1994;71:782-87.
8. Kim KM, Trump BF. Amorphous calcium precipitates in human aortic valve. Calcif Tiss Res 1975;18:155-60.
9. Kim KM Calcification of matrix vesicles in human aortic valve and aortic media. Fed Proc 1976;35:156-62.
10. Dmitrovsky E, Boskey AL. Calcium-acidic phospholipid-phosphate complexes in human atherosclerotic aortas. Calcif Tissue Int 1985;37:121-25.
11. Ortolani F, Petrelli L, Tubaro F, Spina M, Marchini M. Novel ultrastructural features as revealed by phthalocyanine reactions indicate cell priming for calcification in subdermally implanted aortic valves. Connect Tissue Res 2002a;43:44-55.
12. Ortolani F, Tubaro F, Petrelli L, Gandaglia A, Spina M, Marchini M. Copper retention, calcium release and ultrastructural evidence indicate specific Cuprolinic Blue uptake and peculiar modifications in mineralizing aortic valves. Histochem J 2002b;34:41-50.
13. Ortolani F, Petrelli L, Nori SL, Gerosa G, Spina M, Marchini M. Malachite green and phthalocyanine-silver reactions reveal acidic phospholipid involvement in calcifi-

cation of porcine aortic valves in rat subdermal model. Histol Histopathol 2003;18:1131-40.
14. Ortolani F, Bonetti A, Tubaro F, Petrelli L, Contin M, Nori SL et al. Ultrastructural characterization of calcification onset and progression in subdermally implanted aortic valves. Histochemical and spectrometric data. Histol Histopathol 2007;22:261-72.
15. Ortolani F, Rigonat L, Bonetti A, Contin M, Tubaro F, Rattazzi M et al. Pro-calcific responses by aortic valve interstitial cells in a novel in vitro model simulating dystrophic calcification. Ital J Anat Embryol 2010;115:135-39.
16. Bonetti A, Della Mora A, Contin M, Tubaro F, Marchini M, Ortolani F. Ultrastructural and spectrophotometric study on the effects of putative triggers on aortic valve interstitial cells in in vitro models simulating metastatic calcification. Anat Rec 2012;295:1117-27.
17. Smith WE, Dent G. Modern Raman spectroscopy: a practical approach. Wiley Eds, Chichester, 2005.
18. Römer TJ, Brennan JF 3rd, Fitzmaurice M, Feldstein ML, Deinum G, Myles JL et al. Histopathology of human coronary atherosclerosis by quantifying its chemical composition with Raman spectroscopy. Circulation 1998;97:878-85.
19. Buschman HP, Motz JT, Deinum G, Römer TJ, Fitzmaurice M, Kramer JR et al. Diagnosis of human coronary atherosclerosis by morphology-based Raman spectroscopy. Cardiovasc Pathol 2001;10:59-68.
20. van de Poll SW, Kastelijn K, Bakker Schut TC, Strijder C, Pasterkamp G, Puppels GJ et al. On-line detection of cholesterol and calcification by catheter based Raman spectroscopy in human atherosclerotic plaque ex vivo. Heart 2003;89:1078-82.
21. Mangialardo S, Cottinogli V, Cavaretta E, Salvador L, Postorino P, Maras A. Pathological biominerals: Raman and infrared studies of bioapatite deposits in human heart valves. Appl Spectrosc 2012; 66: 1121-27.
22. Pilarczyk M, Czamara K, Baranska M, Natorska J, Kapusta P, Undas A et al. Calcification of aortic human valves studied in situ by Raman microimaging: following mineralization from small grains to big deposits. J Raman Spectrosc 2013; 44:1222-29.
23. DeGelder J, De Gussem K, Vandenabeele P, Moens L. Reference database of Raman spectra of biological molecules. J Raman Spectrosc 2007;38:1133-47.
24. Penel G, Leroy G, Rey C, Bres E. MicroRaman spectral study of the PO4 and CO3 vibrational modes in synthetic and biological apatites. Calfic Tissue Int 1998; 63:475-81.
25. Rey C, Collins B, Goehl T, Dickson IR, Glimcher M. The carbonate environment in bone mineral: a resolution-enhanced Fourier transform spectroscopy study. Calcif Tissue Int 1989;45:157-64.
26. Mohler ER 3rd, Gannon F, Reynolds C, Zimmerman R, Keane MG, Kaplan FS. Bone formation and inflammation in cardiac valves. Circulation 2001;103:1522-28.
27. Steiner I, Kasparová P, Kohout A, Dominik J. Bone formation in cardiac valves: a histopathological study of 128 cases. Virchows Arch 2007;450:653-57.
28. Olsson M, Thyberg J, Nilsson J. Presence of oxidized low density lipoprotein in nonrheumatic stenotic aortic valves. Arterioscler Thromb Vasc Biol 1999;19: 1218-22.
29. Parker RS. Absorption, metabolism, and transport of carotenoids. FASEB J 1996;10:542-51.
30. Buschman HP, Marple ET, Wach ML, Bennett B, Schut TC, Bruining HA et al. In vivo determination of the molecular composition of artery wall by intravascular Raman spectroscopy. Anal Chem 2000;72: 3771-75.
31. Motz JT, Fitzmaurice M, Miller A, Gandhi SJ, Haka AS, Galindo LH et al. In vivo Raman spectral pathology of human atherosclerosis and vulnerable plaque. J Biomed Opt 2006;11:021003.
32. Kaden JJ, Dempfle CE, Grobholz R, Tran HT, Kiliç R, Sarikoç A et al. Interleukin-1 beta promotes matrix metalloproteinase expression and cell proliferation in calcific aortic valve stenosis. Atherosclerosis 2003;170:205-11.